Cancer Research

Tumor Radiosensitization by Monomethyl Auristatin E: Mechanism of Action and Targeted Delivery

Lisa Buckel[1], Elamprakash N. Savariar[2], Jessica L. Crisp[2], Karra A. Jones[3], Angel M. Hicks[1], Daniel J. Scanderbeg[1], Quyen T. Nguyen[4], Jason K. Sicklick[5], Andrew M. Lowy[5], Roger Y. Tsien[2,6], and Sunil J. Advani[1,7]

Abstract

Intrinsic tumor resistance to radiotherapy limits the efficacy of ionizing radiation (IR). Sensitizing cancer cells specifically to IR would improve tumor control and decrease normal tissue toxicity. The development of tumor-targeting technologies allows for developing potent radiosensitizing drugs. We hypothesized that the anti-tubulin agent monomethyl auristatin E (MMAE), a component of a clinically approved antibody-directed conjugate, could function as a potent radiosensitizer and be selectively delivered to tumors using an activatable cell-penetrating peptide targeting matrix metalloproteinases and RGD-binding integrins (ACPP–cRGD–MMAE). We evaluated the ability of MMAE to radiosensitize both established cancer cells and a low-passage cultured human pancreatic tumor cell line using clonogenic and DNA damage assays. MMAE sensitized colorectal and pancreatic cancer cells to IR in a schedule-and dose-dependent manner, correlating with mitotic arrest. Radiosensitization was evidenced by decreased clonogenic survival and increased DNA double-strand breaks in irradiated cells treated with MMAE. MMAE in combination with IR resulted in increased DNA damage signaling and activation of CHK1. To test a therapeutic strategy of MMAE and IR, PANC-1 or HCT-116 murine tumor xenografts were treated with non-targeted free MMAE or tumor-targeted MMAE (ACPP–cRGD–MMAE). While free MMAE in combination with IR resulted in tumor growth delay, tumor-targeted ACPP-cRGD-MMAE with IR produced a more robust and significantly prolonged tumor regression in xenograft models. Our studies identify MMAE as a potent radiosensitizer. Importantly, MMAE radiosensitization can be localized to tumors by targeted activatable cell-penetrating peptides. *Cancer Res; 75(7); 1376–87. ©2015 AACR.*

Introduction

Locally advanced tumors are commonly treated with combination chemotherapy and radiotherapy. In randomized clinical trials, concurrent chemotherapy–radiotherapy has demonstrated improved local tumor control and overall survival, including gastrointestinal tumors (1–4). A principal rationale for using concurrent chemotherapy with radiotherapy is the ability of chemotherapy drugs to radiosensitize. Radiosensitizers increase ionizing radiation (IR)-mediated DNA damage and tumor cell kill (5–7). To be clinically useful, radiation sensitizers must improve the therapeutic index, that is, the level of sensitization of tumor cells must be greater than that of normal tissue. A major limitation to using more potent radiosensitizers is the inability to deliver such agents specifically to the tumor.

Cell sensitivity to IR varies throughout the cell cycle with G_2–M being the most sensitive phase (8). Chemotherapy drugs such as paclitaxel block cells in G_2–M, function as radiosensitizers, and are used clinically with radiotherapy (9). Monomethyl auristatin E (MMAE) is a synthetic derivative of dolastatin 10 and functions as a potent antimitotic agent by inhibiting tubulin polymerization (10). We therefore tested the ability of MMAE to function as a radiosensitizer. However like many potent antitumor agents, systemic delivery of MMAE is limited by toxicity. When MMAE delivery is tumor restricted by conjugation to a CD30 targeting antibody (brentuximab vedotin), its efficacy becomes clinically apparent for lymphomas (11, 12).

To evaluate the ability of targeted MMAE tumor delivery to radiosensitize tumors, we used activatable cell-penetrating peptide (ACPP) technology. ACPP can function as tumor-targeted delivery vehicles (13–16). MMAE has recently been conjugated to ACPP-cRGD as a therapeutic payload (ACPP–cRGD–MMAE) in murine models of breast cancer (17). ACPPs consist of 4 regions: a polyanionic autoinhibitory domain, a protease-sensitive peptide linker region, a cell-penetrating polycationic peptide, and the

[1]Department of Radiation Medicine and Applied Sciences, University of California San Diego, La Jolla, California. [2]Department of Pharmacology, University of California San Diego, La Jolla, California. [3]Department of Pathology, University of California San Diego, La Jolla, California. [4]Department of Surgery, Division of Head and Neck Surgery, University of California San Diego, La Jolla, California. [5]Division of Surgical Oncology, University of California San Diego, La Jolla, California. [6]Howard Hughes Medical Institute, University of California San Diego, La Jolla, California. [7]Center for Advanced Radiotherapy Technologies, University of California San Diego, La Jolla, California.

Note: Supplementary data for this article are available at Cancer Research Online (http://cancerres.aacrjournals.org/).

Note: L. Buckel and E.N. Savariar contributed equally to this article.

Corresponding Author: Sunil J. Advani, Department of Radiation Medicine and Applied Sciences, Moores Cancer Center, University of California San Diego, 3855 Health Sciences Drive, MC 0843, La Jolla, CA 92093. Phone: 858-822-6046; Fax: 858-822-5568; E-mail: sjadvani@ucsd.edu

doi: 10.1158/0008-5472.CAN-14-1931

©2015 American Association for Cancer Research.

AACR

payload to be delivered. The polycationic cell-penetrating peptide consists of 9 D-arginines (r_9) and the autoinhibitory portion is 9 D-glutamates (e_9). A flexible peptide linker separates these 2 domains. For therapeutic applications, anticancer drugs are the payload conjugated to the polycationic cell-penetrating peptide portion to facilitate their intracellular delivery (17). While the ACPP is intact, the polyanion region prevents adhesion and uptake of the polycationic cell-penetrating peptide plus payload. Upon extracellular protease attack on the linker region, drug-conjugated r_9 is released and taken up by cells, where a second protease in the endocytic pathway releases the drug from the r_9. Tumor-specific activation of ACPP has been achieved by inserting a PLGC(Me)AG linker sequence between the polyanionic and polycationic regions. Cleavage of this peptide linker is dependent on gelatinases, MMP-2 and -9. To augment MMP activity and cleavage of PLGC(Me)AG, the ACPP was designed to co-target RGD-binding integrins. $\alpha_v\beta_3$ integrin binds to the hemopexin domain of MMP-2 and enhances MMP activation (18).

Here, we evaluated the ability of MMAE to radiosensitize tumor cells and to be targeted to tumor xenografts in combination with IR. We show MMAE arrests cells in G_2–M in the 1 to 5 nmol/L range and has an IC_{50} that is >6-fold lower than paclitaxel. Of significance, we demonstrate that in addition to its intrinsic antitumor activity, MMAE sensitized cells to IR. MMAE radiosensitization showed both schedule and dose dependency, with MMAE radiosensitization directly correlating with accumulation of cells in G_2–M. In irradiated cells treated with MMAE, there was decreased clonogenic survival and increased activation of the DNA damage response. We then evaluated a therapeutic strategy of combining MMAE with IR in murine tumor xenograft models. We tested both nontargeted and tumor targeted MMAE delivery in PANC-1 and HCT-116 xenografts. For tumor-targeted delivery, we used ACPP–cRGD–MMAE. Combining ACPP–cRGD–MMAE with IR in either HCT-116 or PANC-1 tumor xenografts resulted in prolonged tumor xenograft regression that was not observed with IR or ACPP–cRGD–MMAE alone. Moreover, the advantage of tumor-targeted MMAE delivery was demonstrated in irradiated tumor xenografts. ACPP–cRGD–MMAE tumor-targeted delivery increased tumor xenograft control compared with free MMAE. Our results lay the foundation to test a therapeutic treatment paradigm in which selective and potent radiosensitization can be achieved with tumor-targeted ACPP.

Materials and Methods

Cells and reagents

Human colorectal HCT-116 (ATCC CCL-247) and pancreatic PANC-1 (ATCC CRL-1469) adenocarcinoma cell lines were directly obtained from ATCC (STR tested) and passaged for less than 6 months following resuscitation. 779E is a limited passage pancreatic adenocarcinoma cell line developed in the Lowy laboratory from patient-derived pancreatic adenocarcinoma xenograft. 779E has been whole-exome sequenced in 2014 for mutational status and also was confirmed to be human origin. The XPA-1 cell line was initially derived from a patient-derived pancreatic xenograft from Johns Hopkins (Baltimore, MD) and provided by the Lowy laboratory. Cells were negative for mycoplasma before use in experiments. Cells were cultured in DMEM supplemented with 10% FBS. For patient-derived pancreatic adenocarcinoma xenografts (PDX), primary tumors from patients were directly

implanted orthotopically into NOD/SCID gamma (NSG) mice and passaged serially by orthotopic re-implantation. Paclitaxel (Sigma) and MMAE (Concortis) were both reconstituted in DMSO. ACPP and ratiometric ACPP peptides were synthesized as previously reported (17, 19).

Cell cycle and apoptosis

Cells were treated with MMAE for 24 hours and then fixed in methanol. Cells were treated with RNAse, stained with propidium iodide (PI), and analyzed by FACS using FlowJo software.

Alamar blue assay

Cells were plated in 96-well plates and exposed to MMAE or paclitaxel for 72 hours and analyzed at 560 nm. For irradiated cells, cells were treated with MMAE overnight followed by 6 Gy.

Clonogenic assay

Cells were treated with MMAE for 24 hours and then irradiated with 0 to 8 Gy. Following IR, cells were replated in drug-free media. Colonies formed over 10 to 14 days and were counted.

Neutral comet assay

Cells were treated for indicated length and doses of MMAE followed by 6 Gy. Cells were harvested 15 minutes after IR and underwent neutral electrophoresis (Trevigen). Comet tails were counted in multiple fields (>60 cells per sample) and analyzed using CometScore (TriTek Corp).

γH2Ax immunostaining

Cells grown on glass coverslips were treated with MMAE overnight and then irradiated. Two hours after IR, cells were fixed, permeabilized, and stained with antibody to γH2Ax. Nuclei were stained with 4′,6-diamidino-2-phenylindole (DAPI). Foci were counted in 6 to 8 high-power fields per group.

Immunoblotting

MMAE- and IR-treated cells were harvested and lysed in RIPA buffer with protease and phosphatase inhibitors (Roche). Thirty micrograms of lysate underwent electrophoresis using 4% to 12% Bis–Tris gels (Life Technologies), transferred to polyvinylidene difluoride (PVDF) membranes, and incubated with indicated primary antibodies (Cell Signaling Technology). Blots were developed by ECL (Pierce).

Tumor xenograft gel zymography

All animal work was done in compliance with the UCSD Institutional Animal Use and Care Committee. Six- to 8-week-old female athymic nu/nu mice (UCSD Animal Care Program) were injected subcutaneously into thighs with 5×10^6 HCT-116 or PANC-1 cells in a 1:1 Matrigel (BD) and PBS solution. After tumors grew to >200 mm^3, the right tumor hindlimb was focally irradiated whereas the remainder of the mouse including the left tumor hindlimb was shielded from IR with custom lead blocking >95% of the dose as verified by dosimeters placed on the mouse. Tumors were excised from animals 1 day after IR. Nonirradiated pancreatic adenocarcinoma PDX tumors were also tested for gelatinase activity. Tris–SDS buffer was added at a ratio of 9 μL buffer per mg of tissue. Tumors were homogenized, centrifuged, and the supernatant diluted 1:1 with PBS. Tris-glycine sample buffer (2×) was added and the samples were run on zymography

gels (Life Technologies). The gels were placed in renaturing buffer and then transferred to developing buffer (Life Technologies).

Immunohistochemistry

Mice were treated with IR or intravenous injection of ACPP–cRGD–MMAE, tumor tissue was harvested, formalin fixed, and paraffin embedded followed by staining with indicated antibodies (Ventana Medical Systems). The primary antibody was used at a 1:250 dilution and was visualized using DAB as a chromagen with the UltraMap system (Ventana Medical Systems).

In vivo tumor xenograft optical imaging

Tumor xenografts were irradiated as described above. One day after IR, mice were anesthetized (1:1 mixture of 100 mg/mL of ketamine and 5 mg/mL of midazolam) and intravenously injected with either fluorescently labeled ratiometric ACPP (Cy5 and Cy7) or ACPP–cRGD–MMAE (Cy5). Animals were imaged using a Maestro Small Animal Imager (CRI) with excitation filter of 620/22 nm and 645 nm long-pass emission filter with dichroic filter tuned to 670 nm. Imaging was done both with skin on and after skin removal to decrease autofluorescence and scattering.

In vivo tumor xenograft experiments

HCT-116 or PANC-1 tumor growth was measured with digital calipers. Tumor volume was calculated using the formula as $\frac{1}{2} \times \text{length} \times \text{width}^2$. Mice were randomized into groups as indicated in Results once the average tumor volume reached >200 mm^3. Free MMAE was injected on an equimolar basis to ACPP–cRGD–MMAE.

Statistical analysis

Unpaired 2-sided *t* tests were performed for IC$_{50}$ and radiosensitization experiments in cell culture. In tumor regression studies, 2-way ANOVA analysis was performed with Tukey multiple comparison group. All statistical analyses were performed using Prism software (GraphPad).

Results

Cytotoxicity of MMAE against tumor cell lines

We first tested the ability of MMAE to block proliferating tumor cells in G$_2$–M. Established tumor cell lines (HCT-116 and PANC-1) were exposed to MMAE for 24 hours and then collected. HCT-116 and PANC-1 cells showed a dose–response accumulation of cells in the G$_2$–M, with PANC-1 cells more sensitive to MMAE than HCT-116 cells (Fig. 1A). MMAE at 5 nmol/L resulted in 50% of HCT-116 cells blocked in G$_2$–M and at 2 nmol/L in PANC-1 cells.

We next compared the cytotoxicity of MMAE to paclitaxel. Tumor cells were exposed to MMAE or paclitaxel for 72 hours and cell viability was assessed. For HCT-116, the IC$_{50}$ values for paclitaxel and MMAE were 10.0 and 1.7 nmol/L (Fig. 1B and D). For PANC-1, the IC$_{50}$ values for paclitaxel and MMAE were 15.1 and 0.6 nmol/L (Fig. 1C and D). We also tested a limited passage human pancreatic tumor cell line, 779E. 779E was more resistant to both antimitotic agents; however, it also showed increased sensitivity to MMAE. The IC$_{50}$ values following paclitaxel or MMAE exposure were 52.0 and 5.6 nmol/L, respectively (Fig. 1D).

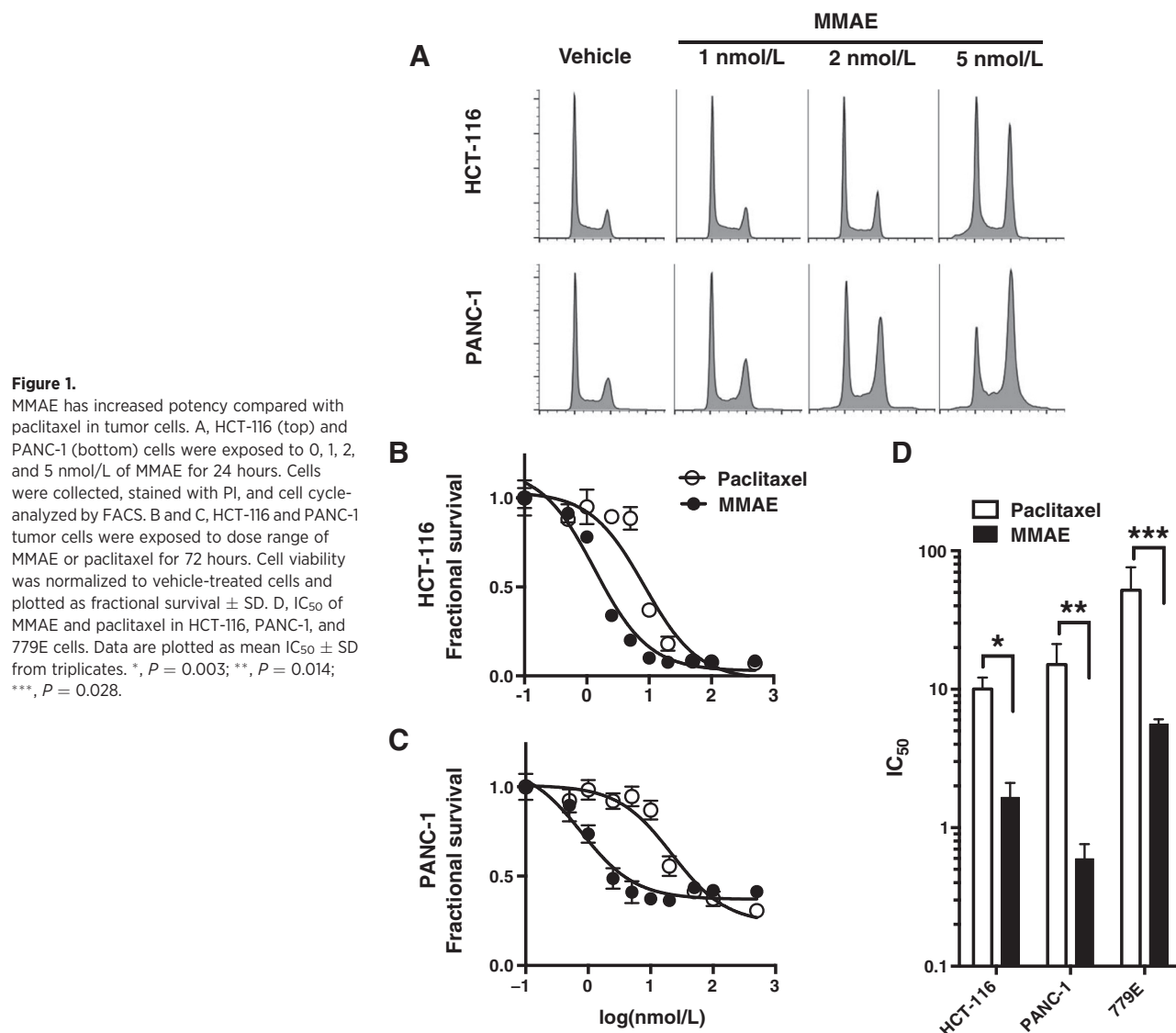### Interaction of MMAE and IR to increase DNA double-strand breaks

Because MMAE blocks cells in the radiosensitive G$_2$–M phase of the cell cycle, we tested whether MMAE specifically interacted with IR. We hypothesized that while a short exposure to MMAE would not influence radiosensitivity, prolonged MMAE exposure with cells accumulating in G$_2$–M would increase sensitivity to IR. DNA double-stand breaks are a hallmark of IR damage and can be measured by neutral comet assay. HCT-116 cells were treated with 5 nmol/L MMAE for varying lengths of time (0, 2, 4, or 24 hours) and then irradiated (Fig. 2A). Irradiation of cell exposed to MMAE for 2 or 4 hours did not increase comet tail length compared with IR alone. However, 24-hour exposure to MMAE significantly increased comet tail length in irradiated cells compared with vehicle or shorter MMAE exposure time. Immunoblotting for cell phase–specific cyclins demonstrated that 24-hour MMAE exposure resulted in the specific accumulation of the G$_2$–M cyclin B compared with nonmitotic cyclins. A similar schedule dependence of MMAE on IR-induced DNA damage was observed in PANC-1 cells (Supplementary Fig. S1A).

Next, we evaluated whether 24-hour exposure to MMAE increased IR-induced DNA breaks in a dose-dependent manner. In irradiated HCT-116 cells, treating with 1 nmol/L MMAE did not increase DNA damage over IR alone. However, 5 nmol/L MMAE resulted in a significant increase in IR-induced DNA double-stranded breaks. These results are concordant with dose–response effects of MMAE on cell cycle in HCT-116 cells, where 1 nmol/L of MMAE did not alter the cell-cycle profile but 5 nmol/L did (Fig. 1A). Overnight MMAE exposure also significantly increased comet tail length following IR in XPA-1 and 779E cells (Supplementary Fig. S1B and S1C).

MMAE decreases clonogenic survival in irradiated cells

Because MMAE increased IR-induced DNA double-strand breaks, we determined whether MMAE decreased survival in irradiated cells. In the first series of experiments, HCT-116 and PANC-1 tumor cell lines were incubated with varying doses of MMAE overnight and then irradiated with 6 Gy the following day. Cells were continuously exposed to MMAE, and tumor cell viability was measured 72 hours after initiation of MMAE treatment. In HCT116 cells, the IC$_{50}$ for MMAE decreased from 1.6 nmol/L for MMAE alone treated cells to 0.8 nmol/L in cells treated with MMAE and IR (Fig. 3A). In PANC-1 cells, a similar relative reduction (~50%) in the IC$_{50}$ of MMAE was observed. In non-irradiated PANC-1 cells, the IC$_{50}$ value for MMAE was 0.8 nmol/L, which decreased to 0.4 nmol/L when IR was combined with MMAE (Fig. 3B).

The primary mode of cell death following IR is mitotic catastrophe. Therefore, we tested the ability of MMAE to decrease clonogenic cell survival. HCT-116 or PANC-1 cells were exposed to MMAE overnight and then irradiated with 0 to 8 Gy. On the basis of the cell-cycle dose response to MMAE from Fig. 1A, we treated HCT-116 cells with 5 nmol/L and PANC-1 cells with 2 nmol/L of MMAE. Following irradiation, cells were replated in drug-free media at low cell density and colonies grew out over 10 to 14 days. Cell-surviving fractions were normalized to 1 for nonirradiated cells treated with either vehicle or MMAE. MMAE resulted in increased tumor cell kill at doses as low as 2 Gy (Fig. 3C and D). Because conventionally fractionated radiotherapy for tumors is often given with 2 Gy concurrently with chemotherapy,

Figure 1.
MMAE has increased potency compared with paclitaxel in tumor cells. A, HCT-116 (top) and PANC-1 (bottom) cells were exposed to 0, 1, 2, and 5 nmol/L of MMAE for 24 hours. Cells were collected, stained with PI, and cell cycle-analyzed by FACS. B and C, HCT-116 and PANC-1 tumor cells were exposed to dose range of MMAE or paclitaxel for 72 hours. Cell viability was normalized to vehicle-treated cells and plotted as fractional survival $\pm$ SD. D, IC_{50} of MMAE and paclitaxel in HCT-116, PANC-1, and 779E cells. Data are plotted as mean $IC_{50} \pm$ SD from triplicates. *, $P = 0.003$; **, $P = 0.014$; ***, $P = 0.028$.

we measured the surviving fraction at 2 Gy (SF2) with varying doses of MMAE. For HCT116, the SF2 for cells treated with 1 nmol/L MMAE was not significantly different from vehicle-treated cells. However, at doses of 2 and 5 nmol/L MMAE, there was a significant reduction in the SF2 compared with cells irradiated with vehicle (Fig. 3E). Consistent with our above results with MMAE alone, irradiated PANC-1 cells showed increased sensitivity at lower MMAE doses. The SF2 in PANC-1 cells was significantly reduced with 1 or 2 nmol/L of MMAE compared with vehicle-treated cells (Fig. 3F).

MMAE increases DNA damage response in irradiated cells

Because MMAE reduced clonogenic cell survival following IR, we tested whether MMAE increased apoptosis in irradiated cells. HCT-116 cells were treated with MMAE for 24 hours followed by IR. Cells were collected 24 hours after IR and the sub-G_1 population (apoptotic) was measured. MMAE alone resulted in a significant increase in apoptosis compared with vehicle-treated cells (Fig. 4A). However, there was no further increase in apoptosis

when IR was combined with MMAE. Because MMAE increased DNA double-strand breaks in irradiated cells (Fig. 2), we then evaluated whether MMAE altered the DNA damage response in irradiated cells. HCT-116 cells were treated with MMAE for 24 hours followed by 6 Gy. Cells were collected 1 hour after IR, and activation of the DNA damage checkpoint proteins CHK1 (pS345) and CHK2 (pT68) was ascertained (Fig. 4B). Interestingly, MMAE enhanced CHK1 activation in irradiated cells, whereas CHK2 activation was not affected. Upon DNA damage, histone H2A becomes phosphorylated at S139, γH2AX. MMAE significantly increased γH2AX foci formation in irradiated HCT-116 and PANC-1 cells (Fig. 4C and D and Supplementary Fig. S2). In nonirradiated cells, MMAE did not alter DNA damage.

Pancreatic and colorectal tumor xenografts express protease activity against PLGC(Me)AG–ACPP peptide linker

While MMAE is a potent cytotoxic molecule in cell culture and an effective radiosensitizer, normal tissue toxicity is a limiting factor to exploit it therapeutically *in vivo*. To target MMAE to

Buckel et al.
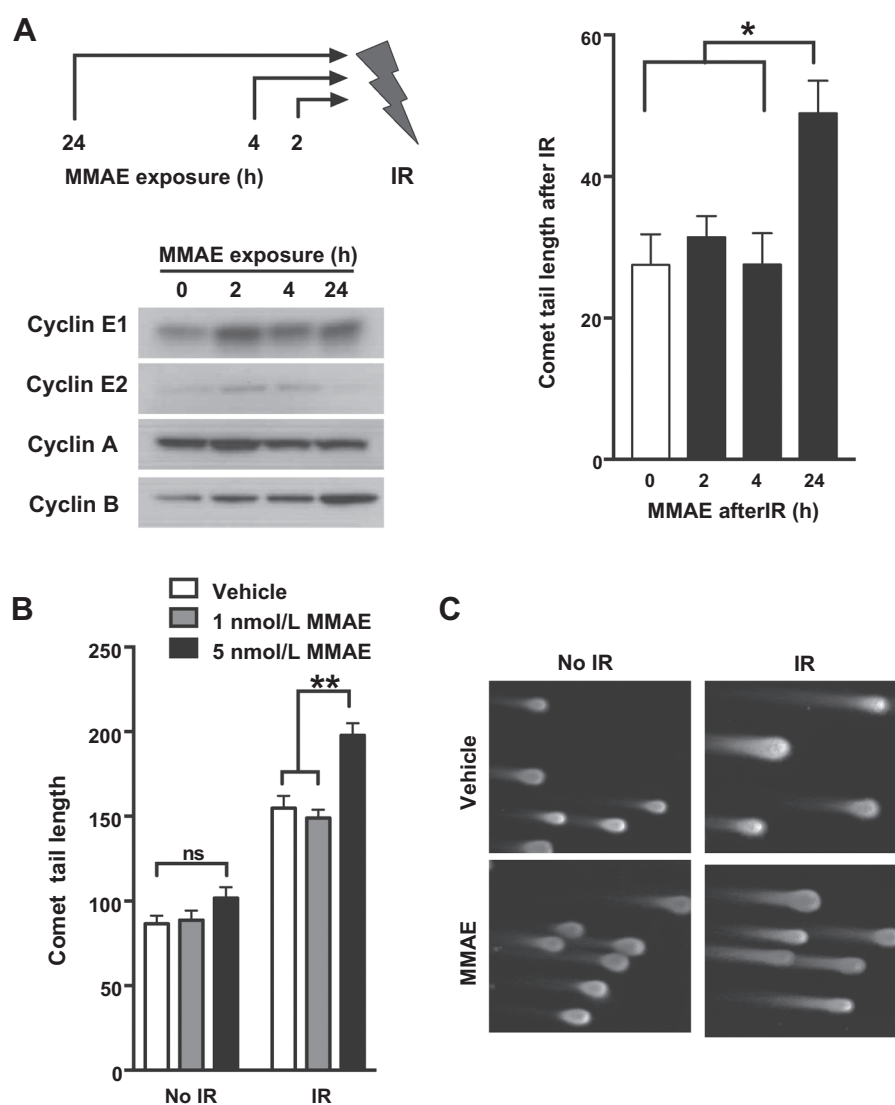
Figure 2.
MMAE increases IR-induced DNA double-strand breaks in a schedule- and dose-dependent manner. A, HCT-116 cells were treated with 5 nmol/L MMAE for 2, 4, or 24 hours followed by 6 Gy. Accumulation of cyclins was assessed by immunoblotting at time of irradiation. Comet tail length was measured using neutral comet assay 15 minutes after IR. Data are plotted as mean comet tail length $\pm$ SEM with nonirradiated comet tail length subtracted. B and C, HCT-116 cells were treated with 0, 1, or 5 nmol/L MMAE for 24 hours and then irradiated with 6 Gy. Comet tail length was measured using neutral comet assay. Data are plotted as mean comet tail length $\pm$ SEM. Representative images from comet tail assay are shown for MMAE dose of 5 nmol/L. *, $P < 0.01$; **, $P < 0.0001$.

tumors, we used MMAE conjugated to a dual integrin and MMP-targeted ACPP, ACPP–cRGD–MMAE (17). The linker region of this ACPP is a substrate for MMP-2 and MMP-9. We first tested whether orthotopically grown patient-derived pancreatic adenocarcinoma xenografts (PDX) expressed MMP activity. Two unique PDX xenografts both contained gelatinase activity (Fig. 5A). Next, we tested whether HCT-116 and PANC-1 tumor xenografts had gelatinase activity. Nonirradiated HCT-116 and PANC-1 tumor lysates both contained gelatinase activity as measured by gel zymography (Fig. 5B). We also tested whether tumor irradiation altered MMP activity. Tumor xenografts were irradiated with a single dose of 6 Gy and harvested the following day. Irradiation of tumors did not hamper gelatinase activity. Because ACPP–cRGD–MMAE is co-targeted to cRGD-binding integrin $\alpha_v\beta_3$, we analyzed β_3 integrin expression and found that PANC-1 and HCT-116 tumors expressed β_3 integrin (Fig. 5C and Supplementary Fig. S3). One day after IR, irradiated tumors also abundantly expressed β_3 integrin.

To directly assess whether HCT-116 and PANC-1 tumor xenografts can cleave the PLGC(Me)AG linker region incorporated into ACPP–cRGD–MMAE, we used a ratiometric ACPP probe with the same MMP substrate sequence (19). Ratiometric ACPP has a Cy5 far red fluorescent donor and Cy7 near-infrared fluorescent acceptor. While intact, the peptide will favor Cy7 re-emission when excited with Cy5 excitation wavelengths, resulting in a low Cy5:Cy7 emission ratio (blue pseudocolor). However, when the peptide is cleaved, Cy5 emission is no longer quenched, resulting in a higher Cy5:Cy7 emission ratio (red pseudocolor). Tumors were grown in the bilateral hindlimbs. The right hindlimb tumor–bearing region was irradiated, whereas the left hindlimb tumor was shielded. The following day ratiometric ACPP (10 nmoles) was injected intravenously and mice were imaged 2 hours later. Tumors were imaged *in situ* and after excision. In both HCT-116 and PANC-1 tumors, tumors had increase in Cy5:Cy7 emission ratio compared with surrounding normal tissue, which is indicative of tumor protease activity cleaving the linker region within the ACPP molecule and releasing the polycationic cell penetrating peptide (Fig. 5D and Supplementary Fig. S4A). Irradiation of tumors 1 day before ratiometric ACPP injection did not diminish peptide cleavage compared
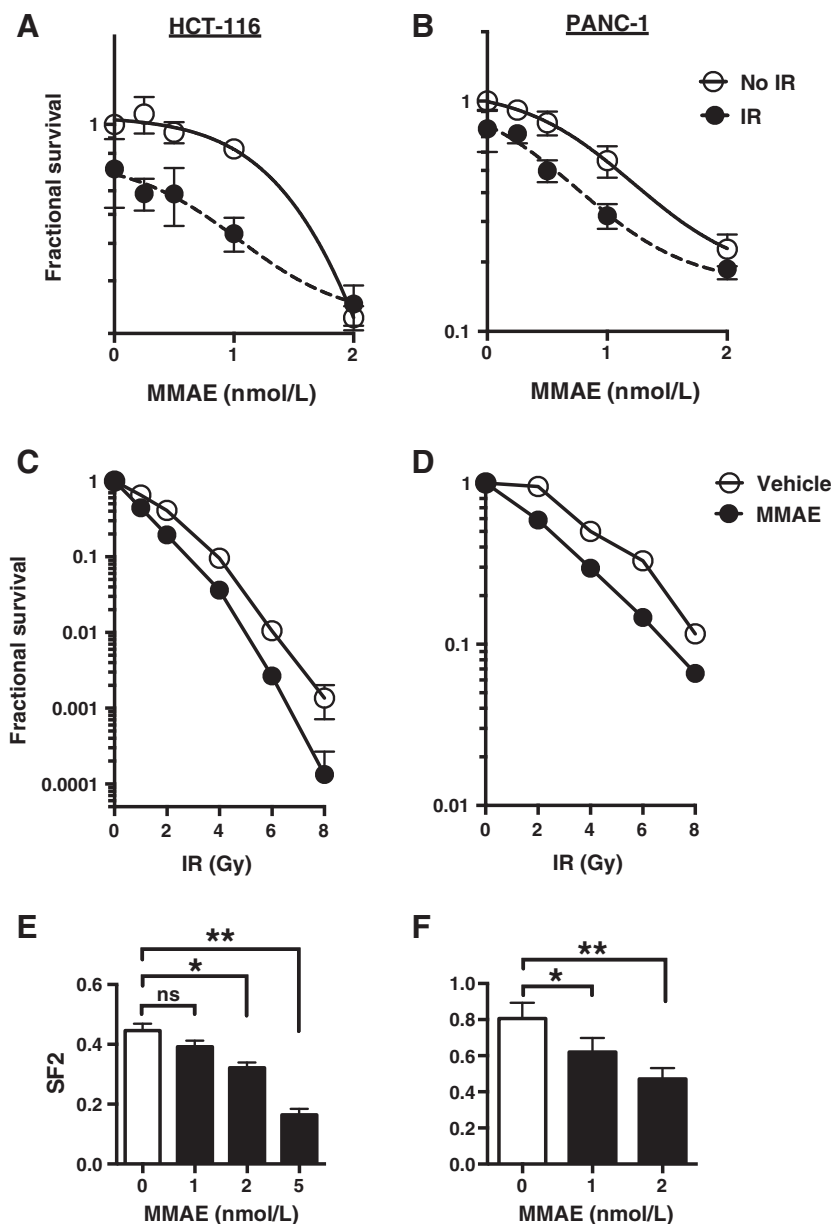
Figure 3.
MMAE decreases clonogenic survival of irradiated tumor cells. A and B, HCT-116 and PANC-1 cells were exposed to varying concentrations of MMAE overnight followed by 6 Gy. Cell viability was normalized to vehicle-treated, nonirradiated cells and plotted as fractional survival $\pm$ SD. C and D, clonogenic survival assay to measure radiosensitization. HCT-116 and PANC-1 cells were treated with 5 and 2 nmol/L MMAE and then irradiated. Data are plotted as mean surviving fraction $\pm$ SD. E and F, the effect of MMAE with 2 Gy on cell survival was measured by clonogenic survival. Survival was normalized to nonirradiated cells for each concentration of MMAE. Data are plotted as mean survival $\pm$ SD. *, $P < 0.01$; **, $P < 0.0001$.

with nonirradiated tumors. Interestingly, there was a trend toward increased Cy5:Cy7 emission ratio in irradiated tumors compared with nonirradiated tumors (Supplementary Fig. S4B).

Therapeutic efficacy of combining an integrin and MMP-targeted ACPP–cRGD–MMAE with IR

We next tested a therapeutic paradigm of using of ACPP-cRGD to deliver the potent radiosensitizer, MMAE. We first validated that MMAE conjugated to the polycationic cell penetrating peptide (r_9) was cytotoxic to tumor cells. HCT-116, PANC-1, and 779E cells were exposed to r_9 alone or r_9 conjugated to MMAE (r_9-MMAE). Carrier r_9 alone had no cytotoxicity, whereas r_9-MMAE produced cytotoxicity in all 3 tumor cell lines (Supplementary Fig. S5). We then tested whether ACPP-cRGD-MMAE accumulated in HCT-116 and PANC-1 tumor xenografts. ACPP-cRGD-MMAE with a Cy5 dye attached to the polycation

region was intravenously injected. Tumors were imaged 6 hours later. As with ratiometric ACPP (Fig. 5D), ACPP–cRGD–MMAE accumulated in both the nonirradiated and irradiated tumor xenografts (Fig. 6A). To determine whether ACPP–cRGD–MMAE delivered functionally active MMAE within the tumor, HCT-116 tumor xenografts were harvested 24 hours following ACPP–cRGD–MMAE intravenous injection and stained for the mitotic marker, pS10 histone H3 (Fig. 6B). In mice intravenously injected with ACPP–cRGD–MMAE, tumor xenografts demonstrated a 32% increase in pS10 histone H3 staining compared with vehicle treatment, $P = 0.002$.

We then evaluated the efficacy of combined MMAE with focal IR to inhibit tumor xenograft growth. First, we tested the hypothesis that MMAE tumor–targeted delivery would increase tumor regression compared with free MMAE delivery (Fig. 6C). PANC-1 tumor xenografts were grown to a mean volume of 200 mm³
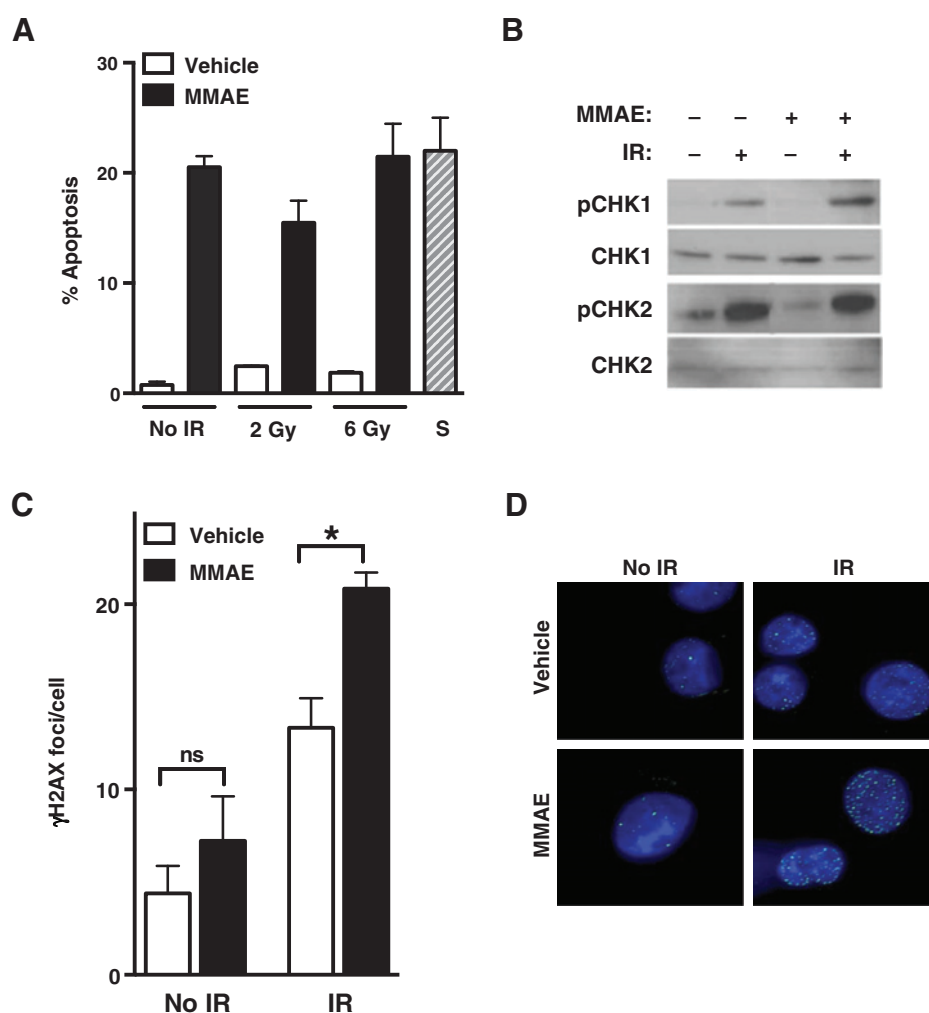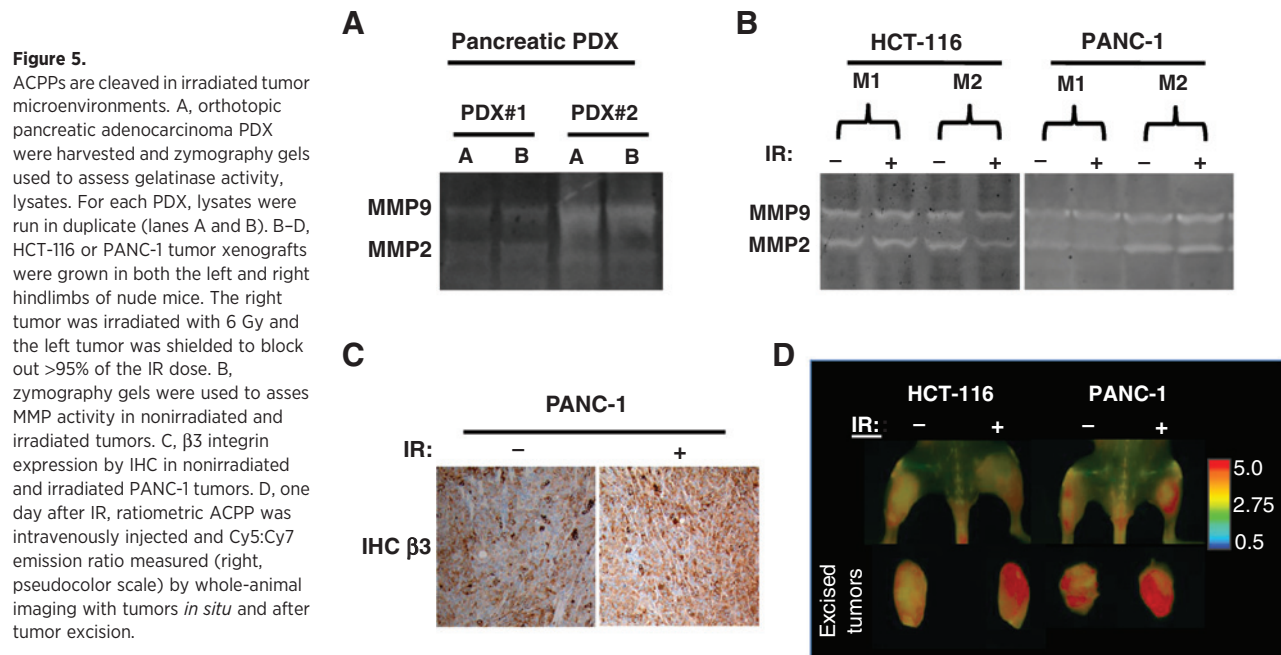
Figure 4.
MMAE increases DNA damage response in irradiated tumor cells. A, HCT-116 cells were treated with MMAE for 24 hours, irradiated, and 24 hours later, apoptosis was measured. Staurosporine-treated cells were used as a positive apoptosis control. B and C, HCT-116 cells were treated with MMAE for 24 hours before 6 Gy and were collected 2 hours later. Lysates were immunoblotted for activation of CHK1 (pS345) and CHK2 (pT68) or cells were fixed and analyzed by immunofluorescence for γH2Ax foci formation. D, representative images of γH2AX foci formation in PANC-1–treated cells (green). Nuclei were stained with DAPI (blue). *, $P < 0.05$.

before initiation of therapy. Free MMAE or ACPP–cRGD–MMAE was intravenously injected on days 0 and 1 (6 nmoles of MMAE/d). This dose of MMAE was chosen based on prior studies on animal toxicity associated with free MMAE delivery. Fractionated IR of 3 Gy per day was given on days 1 and 2. On day 1, when MMAE and IR were both given, IR was delivered in the morning and MMAE in the afternoon. By day 30 following initiation of therapy, free MMAE treatment resulted in a small but statistically significant growth delay of PANC-1 tumors compared with untreated control tumors, $P < 0.0001$. The average tumor volume of free MMAE-treated mice was 75% of untreated controls. More importantly, free MMAE in combination with IR resulted in profound tumor xenograft regression compared with IR or free MMAE alone ($P < 0.0001$). In comparing targeted and free MMAE delivery in the absence of IR, ACPP–cRGD–MMAE resulted in significantly greater tumor regression compared with free MMAE, which is consistent with prior studies involving breast cancer models (17). Of significance, IR combined with ACPP–cRGD–MMAE resulted in prolonged tumor regression when compared with free MMAE and IR ($P < 0.01$). Longer follow-up of tumors demonstrated that 2 of 10 PANC-1 tumors treated with ACPP–cRGD–MMAE and IR were less than or equal to their starting tumor volume on day 0 (Table 1). Of significance, such prolonged and sustained tumor regression was observed with only 2 doses of
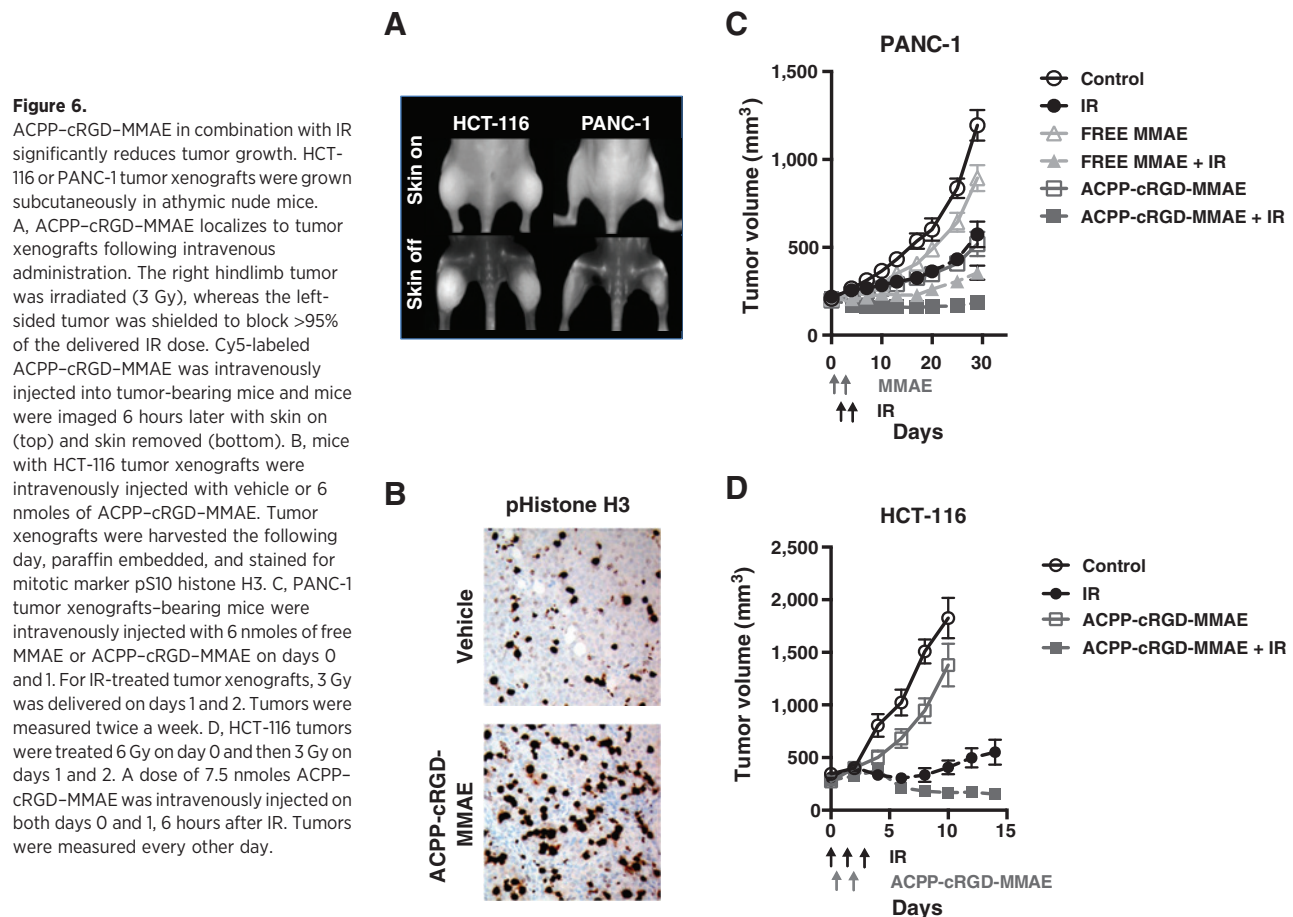
both MMAE and IR and the initial tumor volume was greater than 200 mm³. Moreover, no other treatment group showed long-term tumor regression.

We extended our studies on ACPP–cRGD–MMAE and IR by increasing the dosing schedule to see whether it would result in further improvement in long-term regression. ACPP–cRGD–MMAE was given on days 0, 1, and 2 (6 nmoles/day, 18 nmoles total). Fractionated IR of 3 Gy per day was administered on days 1 to 3. Again on days when ACPP–cRGD–MMAE and IR were both given, IR was delivered in the morning and ACPP–cRGD–MMAE in the afternoon. As we observed in Fig. 6C, combining ACPP–cRGD–MMAE with IR again produced significant tumor regression compared with IR or ACPP–cRGD–MMAE alone treated mice (Supplementary Fig. S6). Tumor volumes in the combined ACPP–cRGD–MMAE and IR mice remained statistically significant compared with all other groups, $P < 0.0001$. More striking and of therapeutic importance, the majority of treated tumors had prolonged tumor regression in PANC-1 tumors upon combining ACPP–cRGD–MMAE with IR. By day 40, none of the control or IR alone treated tumors were smaller than their initial tumor volume on day 0 (Table 1). For the ACPP–cRGD–MMAE alone group, only 1 of 14 tumors was smaller than their initial tumor volumes. In contrast, 8 of 14 tumors in the combined ACPP–cRGD–MMAE and IR group were smaller than their initial tumor volume.

Figure 5.
ACPPs are cleaved in irradiated tumor microenvironments. A, orthotopic pancreatic adenocarcinoma PDX were harvested and zymography gels used to assess gelatinase activity, lysates. For each PDX, lysates were run in duplicate (lanes A and B). B–D, HCT-116 or PANC-1 tumor xenografts were grown in both the left and right hindlimbs of nude mice. The right tumor was irradiated with 6 Gy and the left tumor was shielded to block out >95% of the IR dose. B, zymography gels were used to asses MMP activity in nonirradiated and irradiated tumors. C, β3 integrin expression by IHC in nonirradiated and irradiated PANC-1 tumors. D, one day after IR, ratiometric ACPP was intravenously injected and Cy5:Cy7 emission ratio measured (right, pseudocolor scale) by whole-animal imaging with tumors in situ and after tumor excision.

We then tested a modified treatment schedule of ACPP–cRGD–MMAE and IR using HCT-116 tumor xenografts. HCT-116 tumors were grown to mean tumor volume of >270 mm³ before initiation of therapy. We had observed that 6 Gy given to HCT-116 xenografts improved ratiometric ACPP probe cleavage (Fig. 5D and Supplementary Fig. S4). Therefore in irradiated tumors, we

Figure 6.
ACPP–cRGD–MMAE in combination with IR significantly reduces tumor growth. HCT-116 or PANC-1 tumor xenografts were grown subcutaneously in athymic nude mice. A, ACPP–cRGD–MMAE localizes to tumor xenografts following intravenous administration. The right hindlimb tumor was irradiated (3 Gy), whereas the left-sided tumor was shielded to block >95% of the delivered IR dose. Cy5-labeled ACPP–cRGD–MMAE was intravenously injected into tumor-bearing mice and mice were imaged 6 hours later with skin on (top) and skin removed (bottom). B, mice with HCT-116 tumor xenografts were intravenously injected with vehicle or 6 nmoles of ACPP–cRGD–MMAE. Tumor xenografts were harvested the following day, paraffin embedded, and stained for mitotic marker pS10 histone H3. C, PANC-1 tumor xenografts–bearing mice were intravenously injected with 6 nmoles of free MMAE or ACPP–cRGD–MMAE on days 0 and 1. For IR-treated tumor xenografts, 3 Gy was delivered on days 1 and 2. Tumors were measured twice a week. D, HCT-116 tumors were treated 6 Gy on day 0 and then 3 Gy on days 1 and 2. A dose of 7.5 nmoles ACPP–cRGD–MMAE was intravenously injected on both days 0 and 1, 6 hours after IR. Tumors were measured every other day.

Table 1. Sustained tumor growth inhibition following treatment with ACPP–cRGD–MMAE and IR

	$V(end)/V(0) \leq 1$		
	PANC-1, expt 1	PANC-1, expt 2	HCT-116
Control	0%	0%	0%
IR	0%	0%	30%
Free MMAE	0%	—	—
Free MMAE + IR	0%	—	—
ACPP–cRGD–MMAE	0%	7%	0%
ACPP–cRGD–MMAE + IR	20%	57%	90%

NOTE: The percentage of treated PANC-1 and HCT-116 tumor xenografts at days 30, 40, 14 [PANC-1 (Fig. 5B), PANC-1 (Supplementary Fig. S5), HCT-116 (Fig. 5C), respectively] after initiation of treatment were smaller than the initial tumor volume on day 0, $V(end)/V(0) \leq 1$.

delivered 6 Gy on day 0 followed by 3 Gy on days 1 and 2. ACPP–cRGD–MMAE was intravenously injected on days 0 and 1, 6 hours following irradiation (7.5 nmoles/day). The dose of ACPP–cRGD–MMAE was increased compared with PANC-1, as HCT-116 cells had a higher IC_{50} for MMAE. As seen in PANC-1 tumors, ACPP–cRGD–MMAE alone produced a modest growth delay compared with untreated control tumors (Fig. 6D). As expected, IR alone resulted in an initial tumor growth delay (especially prominent due to the 6 Gy dose on day 0); however by day 10, tumor volume began to increase. Combining ACPP–cRGD–MMAE with IR again produced sustained tumor regression compared with IR alone starting at day 10 after the initiation of therapy, $P < 0.006$. By day 14, none of the control or ACPP–RGD–MMAE–treated tumors were smaller than their initial tumor volume on day 0 (Table 1). For the IR alone group, only 3 of 10 tumors were smaller than their initial tumor volume. In contrast, 9 of 10 tumors in the combined ACPP–cRGD–MMAE and IR group were smaller than their initial tumor volume.

Discussion

In these series of studies, we have identified that MMAE can radiosensitize tumor cells and enhance tumor xenograft regression in combination with IR. Moreover, we tested a therapeutic paradigm whereby a potent radiosensitizer such as MMAE can be selectively delivered to tumors using ACPP to increase tumor response to IR (Supplementary Fig. S7). MMAE, a synthetic derivative of dolastatin 10, sensitizes cancer cells to IR-mediated DNA damage and cell kill (10). Intrinsic tumor cell resistance to IR is dependent on a multitude of factors, including activity of DNA repair pathways, tumor oxygenation status, and the cell cycle (5–7). By pharmacologically targeting these pathways, cells become more sensitive to the effects of IR. An optimal cancer therapeutic agent would have the dual benefit of single-agent potent tumoricidal activity and also sensitize tumors to IR. Our data support MMAE as a candidate that meets such requirements.

MMAE has previously been shown to have single-agent antitumor efficacy against a broad panel of tumor histologies when appropriately delivered (17, 20, 21). In our own studies with established cancer cells and a limited patient passage patient-derived pancreatic adenocarcinoma cell line, MMAE had an IC_{50} that is at least 6-fold lower than paclitaxel (Fig. 1). MMAE is an anti-tubulin agent that blocks cells in G_2–M, and the G_2–M phase of the cell cycle is the most sensitive to the IR (8). We demonstrated that MMAE increased IR induced DNA double-strand breaks in both a schedule- and a dose-dependent manner that directly correlated with the accumulation of cells in G_2–M (Figs. 1

and 2). MMAE also decreased clonogenic survival of pancreatic and colorectal cancer cells in the 1 to 5 nmol/L range in combination with IR indicative of its application as a potent radiosensitizer. Mechanistically, MMAE increased clonogenic cell death in irradiated cells. The decreased cell survival following combined IR and MMAE was not due to apoptosis, suggesting mitotic catastrophe as the cause of MMAE enhanced cell death in irradiated cells. In support of this, MMAE enhanced the DNA damage response pathway in irradiated cells. Both γH2AX foci formation and activation of CHK1 were increased in cells treated with MMAE before irradiation. Understanding the cellular response to MMAE can allow for future rational drug combinations with MMAE to further augment radiosensitization by inhibiting survival pathways induced by MMAE.

While MMAE is a potent radiosensitizer *in vitro*, it requires tumor-targeted delivery to achieve a clinically meaningful therapeutic index in *vivo*. We have therefore initially evaluated a strategy using MMP and cRGD-binding integrin targeted ACPP delivery of MMAE in combination with focal IR (17). A major limitation to the therapeutic use of radiosensitizers is the lack of tumor-specific delivery (22, 23). Radiosensitizer delivery that is nontargeted can result in increased radiosensitization of not only tumor cells but also surrounding normal tissue. This results in no net gain in the therapeutic index of radiotherapy. Previous reports have tested nanoparticles as radiosensitizer delivery vehicles (24–27). Here, we have demonstrated the efficacy of ACPP technology to deliver the potent radiosensitizer MMAE specifically to tumors. Following MMP-2/-9 and $\alpha_v\beta_3$ integrin targeted delivery and release of MMAE conjugated cell-penetrating peptide from the ACPP, tumor xenografts demonstrated prolonged regression in combination with IR compared with nontargeted free MMAE delivery (Fig. 6 and Table 1). Moreover at equimolar systemic intravenous injection, ACPP–cRGD–MMAE improved tumor xenograft regression when compared with nontargeted MMAE for both nonirradiated and irradiated tumors. We also tested altering the order of delivery of IR and ACPP–cRGD–MMAE. In the PANC-1 xenograft experiments, ACPP–cRGD–MMAE was initially injected 1 day before 3 Gy fractions of IR (Fig. 6 and Supplementary Fig. S6). These experiments were designed on the basis of MMAE functioning as a radiosensitizer by blocking tumor cells in G_2–M. Therefore, MMAE was injected into mice before irradiation. To test the ability of IR to modulate the tumor environment and increase ACPP–cRGD–MMAE tumor accumulation, we altered the treatment scheduling, with a larger 6 Gy dose given 1 day before ACPP–cRGD–MMAE injection in HCT-116 xenografts (Fig. 6D). The rationale for an initial 6 Gy in the HCT-116 tumor xenograft experiment was 2-fold. First, HCT-116 tumors grow more rapidly in our tumor model compared with PANC-1 tumor xenografts. Second, a dose of 6 Gy increased ratiometric ACPP activation in irradiated tumors compared with nonirradiated tumors (Fig. 5D and Supplementary Fig. S4). Therefore, we hypothesized that pre-irradiation would increase ACPP-mediated delivery of MMAE to irradiated tumor xenografts. Following the initial 6 Gy dose to increase ACPP-mediated MMAE delivery, 2 doses of 3 Gy were given after ACPP–cRGD–MMAE. Even with a total dose delivered of 12 Gy to HCT-116 tumors over 3 days, the majority of HCT-116 tumors began to regrow in contrast to combined treatment with ACPP–cRGD–MMAE. While the treatment regimens in the 3 xenograft experiments varied from each other, a strength is that their conclusions consistently

demonstrated that combining ACPP–cRGD–MMAE with IR resulted in sustained tumor xenograft regression (Table 1).

ACPP-conjugated delivery of radiosensitizers is innovative and of clinical significance in that it offers a solution to the problem of nonselective radiosensitization of molecules for not only cancer cells but also surrounding normal tissue. In addition, it provides a mechanism for efficient intracellular delivery and release of the conjugated drug payload, that is, MMAE. MMAE is conjugated to the polycationic cell-penetrating peptide portion of ACPP through a cathepsin B–sensitive linker (valine–citrulline; ref. 17). Once the ACPP peptide linker is cleaved in the tumor microenvironment, the cell-penetrating peptide MMAE is internalized and free MMAE released from lysosomes through the action of cathepsin B. Such a therapeutic paradigm can allow for the clinical development and testing of more potent radiosensitizers, as systemic toxicity and collateral normal tissue damage would be decreased. Because MMP activity is high in the tumor microenvironment, MMP-2/-9–targeted ACPP may also be a broadly applicable tumor-selective delivery vehicle for radiosensitizers. Meanwhile, the only immediately clinically approved vehicle for MMAE delivery is brentuximab vedotin, with a host of similar antibody–MMAE conjugates undergoing clinical trial (11, 28). Our results showing radiosensitization by free MMAE *in vitro* suggest that antibody–MMAE conjugates should show similar radiosensitization, as the antibody is another mechanistic targeting vector for MMAE. Viewed another way, IR may be a valuable adjunct to chemotherapy with antibody–drug conjugates.

Our work also lays the foundation for further refinement of radiation-guided ACPP delivery of potent tumoricidal and radiosensitizing agents. IR results in changes in the tumor microenvironment including alterations of tumor permeability and retention, gene expression, tumor cell surface receptor expression, and protease activity. The physics of IR allows for IR to be specifically deposited to tumor tissue and can allow it to serve as beaconing mechanism for systemically delivered therapeutic agents. Such a concept has been seen with combining IR with oncolytic viruses, where IR enhances the ability of both intratumoral and systemically delivered oncolytic viruses to replicate in irradiated tumor microenvironment (29–32). IR has also been used to induce the expression of neoantigens within tumors that can function as receptors for peptide ligand–targeted nanoparticles (33–36). Interestingly, MMP activity has been reported to be induced in irradiated tumors, including patient-derived rectal cancers (37–40). Moreover, the cRGD-binding integrin $\alpha_v\beta_3$ expression is also upregulated by IR and modulates cell response to IR (41–44). While gelatin zymography of excised tumor xenografts did not reveal an increase in gelatinase activity in irradiated tumors compared with their nonirradiated counterparts, ratiometric PLGC(Me)AG linker ACPP showed a trend toward increase Cy5:Cy7 emission ratio in irradiated tumor xenografts compared with nonirradiated tumor xenografts (Fig. 5 and Supplementary Fig. S4). Our ratiometric PLGC(Me)AG linker ACPP contains both Cy5 (polycationic side) and Cy7 (polyanionic side), and real-time ratiometric monitoring of tumors in mice has demonstrated tumor-specific cleavage of this ratiometric probe (19). While Cy5 has increased tissue attenuation than Cy7, in our experience, the greater extinction coefficient, quantum yield, and chemical stability of Cy5 compared with Cy7 make up for the somewhat greater attenuation (45). In addition, we have not found a ratiometric FRET donor–acceptor pair in which the donor is Cy7 and the acceptor is about 100 nm longer in wavelength.

An alternative explanation for the enhanced accumulation of ACPP within irradiated tumors as opposed to nonirradiated tumors is the concept of enhanced permeability and retention (EPR) of systemically delivered macromolecular agents of ≥40 kDa (46–48). IR has been shown to decrease the tumor interstitial pressure, especially with delivery of doses >10 Gy. By decreasing tumor interstitial pressure, IR can augment diffusion of macromolecular drugs into the tumor. However, the ACPP–cRGD–MMAE is only 6.9 KDa, so it may not be affected as much by EPR. Using ratiometric ACPP probes, further optimization of radiation dose fraction schedule may improve cleavage and activation of ACPP through increased expression of cRGD-binding integrins and MMP-2/-9 activity or increased tumor EPR (Fig. 5 and Supplementary Fig. S4). Moreover, a radiation ACPP could be engineered in which a flexible peptide linker region could be inserted that is cleaved by IR-induced tumor protease activity. This would increase ACPP cleavage dependence upon IR-induced microenvironment proteases (Supplementary Fig. S7). Our results provide a conceptual basis for IR-controlled ACPP to be developed that could deliver potent radiosensitizers. In such a treatment paradigm, there would be preferential accumulation of the radiosensitizer with the irradiated tumor and reduced bioavailability of the radiosensitizer to normal tissue. Such technology is not limited to radiosensitizer delivery. IR could be used to induce a "proteolytic switch" in the irradiated tumor target microenvironment to facilitate localized delivery of systemically administered cytotoxic antitumor agents.

Disclosure of Potential Conflicts of Interest

Authors' Contributions

Conception and design: E.N. Savariar, J.L. Crisp, R.Y. Tsien, S.J. Advani
Development of methodology: E.N. Savariar, R.Y. Tsien
Acquisition of data (provided animals, acquired and managed patients, provided facilities, etc.): L. Buckel, E.N. Savariar, J.L. Crisp, K.A. Jones, A.M. Hicks, D.J. Scanderbeg, J.K. Sicklick, A.M. Lowy, S.J. Advani
Analysis and interpretation of data (e.g., statistical analysis, biostatistics, computational analysis): L. Buckel, E.N. Savariar, J.L. Crisp, K.A. Jones, S.J. Advani
Writing, review, and/or revision of the manuscript: L. Buckel, E.N. Savariar, J.L. Crisp, Q.T. Nguyen, J.K. Sicklick, A.M. Lowy, R.Y. Tsien, S.J. Advani
Administrative, technical, or material support (i.e., reporting or organizing data, constructing databases): L. Buckel, D.J. Scanderbeg
Study supervision: R.Y. Tsien, S.J. Advani

Acknowledgments

Grant Support

Buckel et al.

and R.Y. Tsien), the American Cancer Society IRG #70-002 (S.J. Advani), University of California Cancer Research Coordinating Committee (S.J. Advani), and UCSD Academic Senate (S.J. Advani).

The costs of publication of this article were defrayed in part by the payment of page charges. This article must therefore be hereby marked *advertisement* in accordance with 18 U.S.C. Section 1734 solely to indicate this fact.

Received June 30, 2014; revised February 2, 2015; accepted February 4, 2015; published OnlineFirst February 13, 2015.

References

1. Werner J, Combs SE, Springfeld C, Hartwig W, Hackert T, Büchler MW. Advanced-stage pancreatic cancer: therapy options. Nat Rev Clin Oncol 2013;10:323–33.
2. Gutt R, Liauw SL, Weichselbaum RR. The role of radiotherapy in locally advanced pancreatic carcinoma. Nat Rev Gastroenterol Hepatol 2010;7: 437–47.
3. Aklilu M, Eng C. The current landscape of locally advanced rectal cancer. Nat Rev Clin Oncol 2011;8:649–59.
4. Pretz JL, Wo JY, Mamon HJ, Kachnic LA, Hong TS. Chemoradiation therapy: localized esophageal, gastric, and pancreatic cancer. Surg Oncol Clin N Am 2013;22:511–24.
5. Moding EJ, Kastan MB, Kirsch DG. Strategies for optimizing the response of cancer and normal tissues to radiation. Nat Rev Drug Discov 2013;12:526–42.
6. Liauw SL, Connell PP, Weichselbaum RR. New paradigms and future challenges in radiation oncology: an update of biological targets and technology. Sci Transl Med 2013;5:173sr2.
7. Raleigh DR, Haas-Kogan DA. Molecular targets and mechanisms of radio-sensitization using DNA damage response pathways. Future Oncol 2013; 9:219–23.
8. Terasima T, Tolmach LJ. Variations in several responses of HeLa cells to x-irradiation during the division cycle. Biophys J 1963;3:11–33.
9. Tishler RB, Schiff PB, Geard CR, Hall EJ. Taxol: a novel radiation sensitizer. Int J Radiat Oncol Biol Phys 1992;122:613–7.
10. Bai R, Pettit GR, Hamel E. Dolastatin 10, a powerful cytostatic peptide derived from a marine animal. Inhibition of tubulin polymerization mediated through the vinca alkaloid binding domain. Biochem Pharmacol 1990;39:1941–49.
11. Doronina SO, Toki BE, Torgov MY, Mendelsohn BA, Cerveny CG, Chace DF, et al. Development of potent monoclonal antibody auristatin con-jugates for cancer therapy. Nat Biotechnol 2003;21:778–84.
12. Sievers EL, Senter PD. Antibody-drug conjugates in cancer therapy. Annu Rev Med 2013;64:15–29.
13. Jiang T, Olson ES, Nguyen QT, Roy M, Jennings PA, Tsien RY. Tumor imaging by means of proteolytic activation of cell-penetrating peptides. Proc Natl Acad Sci U S A 2004;101:17867–72.
14. Aguilera TA, Olson ES, Timmers MM, Jiang T, Tsien RY. Systemic *in vivo* distribution of activatable cell penetrating peptides is superior to that of cell penetrating peptides. Integr Biol (Camb) 2009;1:371–81.
15. Olson EA, Aguilera TA, Jiang T, Ellies LG, Nguyen QT, Wong EH, et al. *In vivo* characterization of activatable cell penetrating peptides for targeting pro-tease activity in cancer. Integr Biol (Camb) 2009;1:382–93.
16. Whitney M, Crisp JL, Olson ES, Aguilera TA, Gross LA, Ellies LG, et al. Parallel *in vivo* and *in vitro* selection using phage display identifies protease-dependent tumor-targeting peptides. J Biol Chem 2010;285: 22532–41.
17. Crisp JL, Savariar EN, Glasgow HL, Ellies LG, Whitney MA, Tsien RY. Synergistic targeting of integrin avb3 and matrix metalloproteinase-2 improves optical imaging of tumors and chemotherapeutic efficiency. Mol Cancer Therapeutics 2014;13:1514–25.
18. Deryugina EI, Ratnikov B, Monosov E, Postnova TI, DiScipio R, Smith JW, et al. MT1-MMP initiates activation of pro-MMP-2 and integrin alphav-beta3 promotes maturation of MMP-2 in breast carcinoma cells. Exp Cell Res 2001;263:209–23.
19. Savariar EN, Felsen CN, Nashi N, Jiang T, Ellies LG, Steinbach P, et al. Real-time *in vivo* molecular detection of primary tumors and metastases with ratiometric activatable cell-penetrating peptides. Cancer Res 2013; 73:855–64.
20. Ma D, Hopf CE, Malewicz AD, Donovan GP, Senter PD, Goeckeler WF, et al. Potent antitumor activity of an auristatin-conjugated, fully human mono-clonal antibody to prostate-specific membrane antigen. Clin Cancer Res 2006;12:2591–6.
21. Breij EC, de Goeij BE, Verploegen S, Schuurhuis DH, Amirkhosravi A, Francis J, et al. An antibody-drug conjugate that targets tissue factor exhibits potent therapeutic activity against a broad range of solid tumors. Cancer Res 2014;74:1214–26.
22. Liu FF, Okunieff P, Bernhard EJ, Stone HB, Yoo S, Coleman CN, et al. Lessons learned from radiation oncology trials. Clin Cancer Res 2013;19: 6089–100.
23. Lin SH, George TJ, Ben-Josef E, Bradley J, Choe KS, Edelman MJ, et al. Opportunities and challenges in the era of molecularly targeted agents and radiation therapy. J Natl Cancer Inst 2013;105:686–93.
24. Miller SM, Wang AZ. Nanomedicine in chemoradiation. Ther Deliv 2013;4: 239–50.
25. Werner ME, Cummings ND, Sethi M, Wang EC, Sukumar R, Moore DT, et al. Preclinical evaluation of Genexol-PM, a nanoparticle formulation of paclitaxel, as a novel radiosensitizer for the treatment of non-small cell lung cancer. Int J Radiat Oncol Biol Phys 2013;86:463–8.
26. Joh DY, Sun L, Stangl M, Al Zaki A, Murty S, Santoiemma PP, Davis JJ, et al. Selective targeting of brain tumors with gold nanoparticle-induced radio-sensitization. PLoS One 2013;8:e62425.
27. Wang Y, Mo L, Wei W, Shi X. Efficacy and safety of dendrimer nanoparticles with coexpression of tumor necrosis factor-α and herpes simplex virus thymidine kinase in gene radiotherapy of the human uveal melanoma OCM-1 cell line. Int J Nanomedicine 2013;8:3805–16.
28. Mullard A. Maturing antibody-drug conjugate pipeline hits 30. Nat Rev Drug Discov 2013;12:329–32.
29. Hallahan DE, Mauceri HJ, Seung LP, Dunphy EJ, Wayne JD, Hanna NN, et al. Spatial and temporal control of gene therapy using ionizing radiation. Nat Med 1995;1:786–91.
30. Mezhir JJ, Advani SJ, Smith KD, Darga TE, Poon AP, Schmidt H, et al. Ionizing radiation activates late herpes simplex virus 1 promoters via the p38 pathway in tumors treated with oncolytic viruses. Cancer Res 2005; 65:9479–84.
31. Advani SJ, Markert JM, Sood RF, Samuel S, Gillespie GY, Shao MY, et al. Increased oncolytic efficacy for high-grade gliomas by optimal integration of ionizing radiation into the replicative cycle of HSV-1. Gene Ther 2011;18:1098–102.
32. Advani SJ, Buckel L, Chen NG, Scanderbeg DJ, Geissinger U, Zhang Q, et al. Preferential replication of systemically delivered oncolytic vaccinia virus in focally irradiated glioma xenografts. Clin. Cancer Res 2012;18: 2579–90.
33. Hallahan DE, Qu S, Geng L, Cmelak A, Chakravarthy A, Martin W, et al. Radiation-mediated control of drug delivery. Am J Clin Oncol 2001;24: 473–80.
34. Hallahan D, Geng L, Qu S, Scarfone C, Giorgio T, Donnelly E, et al. Integrin-mediated targeting of drug delivery to irradiated tumor blood vessels. Cancer Cell 2003;3:63–74.
35. Hariri G, Yan H, Wang H, Han Z, Hallahan DE. Radiation-guided drug delivery to mouse models of lung cancer. Clin Cancer Res 2010;16: 4968–77.
36. Passarella RJ, Spratt DE, van der Ende AE, Phillips JG, Wu H, Sathiyakumar V, et al. Targeted nanoparticles that deliver a sustained, specific release of Paclitaxel to irradiated tumors. Cancer Res 2010;70:4550–9.
37. Fujita M, Otsuka Y, Yamada S, Iwakawa M, Imai T. X-ray irradiation and Rho-kinase inhibitor additively induce invasiveness of the cells of the pancreatic cancer line, MIAPaCa-2, which exhibits mesenchymal and amoeboid motility. Cancer Sci 2011;102:792–8.
38. Lee WH, Warrington JP, Sonntag WE, Lee YW. Irradiation alters MMP-2/TIMP-2 system and collagen type IV degradation in brain. Int J Radiat Oncol Biol Phys 2012;82:1559–66.
39. Speake WJ, Dean RA, Kumar A, Morris TM, Scholefield JH, Watson SA. Radiation induced MMP expression from rectal cancer is short lived but contributes to *in vitro* invasion. Eur J Surg Oncol 2005;31:869–74.

40. Kumar A, Collins HM, Scholefield JH, Watson SA. Increased type-IV collagenase (MMP-2 and MMP-9) activity following preoperative radiotherapy in rectal cancer. Br J Cancer 2000;82:960–5.

41. Xu W, Luo T, Li P, Zhou C, Cui D, Pang B, et al. RGD-conjugated gold nanorods induce radiosensitization in melanoma cancer cells by downregulating $\alpha(v)\beta3$ expression. Int J Nanomedicine 2012;7: 915–24.

42. Abdollahi A, Griggs DW, Zieher H, Roth A, Lipson KE, Saffrich R, et al. Inhibition of alpha(v)beta3 integrin survival signaling enhances antiangiogenic and antitumor effects of radiotherapy. Clin Cancer Res 2005;11:6270–79.

43. Egami T, Ohuchida K, Yasui T, Mizumoto K, Onimaru M, Toma H, et al. Up-regulation of integrin beta3 in radioresistant pancreatic cancer impairs adenovirus-mediated gene therapy. Cancer Sci 2009;100:1902–7.

44. Rieken S, Habermehl D, Mohr A, Wuerth L, Lindel K, Weber K, et al. Targeting $\alpha v\beta3$ and $\alpha v\beta5$ inhibits photon-induced hypermigration of malignant glioma cells. Radiat Oncol 2011;6:132.

45. Nguyen QT, Tsien RY. Fluorescence-guided surgery with live molecular navigation–a new cutting edge. Nat Rev Cancer 2013;13:653–62.

46. Znati CA, Rosenstein M, Boucher Y, Epperly MW, Bloomer WD, Jain RK. Effect of radiation on interstitial fluid pressure and oxygenation in a human tumor xenograft. Cancer Res 1996;56:964–68.

47. Li C, Ke S, Wu QP, Tansey W, Hunter N, Buchmiller LM, et al. Tumor irradiation enhances the tumor-specific distribution of poly(L-glutamic acid)-conjugated paclitaxel and its antitumor efficacy. Clin Cancer Res 2000;6:2829–34.

48. Giustini AJ, Petryk AA, Hoopes PJ. Ionizing radiation increases systemic nanoparticle tumor accumulation. Nanomedicine 2012;8:818–21.

Cancer Research

AACR American Association for Cancer Research

Tumor Radiosensitization by Monomethyl Auristatin E: Mechanism of Action and Targeted Delivery

Lisa Buckel, Elamprakash N. Savariar, Jessica L. Crisp, et al.

Updated version	Access the most recent version of this article at: doi:10.1158/0008-5472.CAN-14-1931
Supplementary Material	Access the most recent supplemental material at: http://cancerres.aacrjournals.org/content/suppl/2015/02/13/0008-5472.CAN-14-1931.DC1.html

Cited Articles	This article cites by 48 articles, 15 of which you can access for free at: http://cancerres.aacrjournals.org/content/75/7/1376.full.html#ref-list-1

E-mail alerts	Sign up to receive free email-alerts related to this article or journal.
Reprints and Subscriptions	To order reprints of this article or to subscribe to the journal, contact the AACR Publications Department at pubs@aacr.org.
Permissions	To request permission to re-use all or part of this article, contact the AACR Publications Department at permissions@aacr.org.